-

Simulation of Boundary-Layer Cumulus and Stratocumulus Clouds Using a Cloud-resolving Model with Low- and Third-order Turbulence Closures

Anning Cheng[1] and Kuan-Man Xu[2]

1. Analytical Services & Materials, Inc., Hampton, VA

2. Climate Science Branch, NASA Langley Research Center, Hampton, VA

Submitted to

Journal of the Meteorological Society of Japan

October 5, 2007

Corresponding author address:
Dr. Kuan-Man Xu
Climate Science Branch
NASA Langley Research Center
Mail Stop 420
Hampton, VA 23681

-

e-mail: Kuan-Man.Xu@nasa.gov

ABSTRACT

The effects of subgrid-scale condensation and transport become more important as the grid spacings increase from those typically used in large-eddy simulation (LES) to those typically used in cloud-resolving models (CRMs). Incorporation of these effects can be achieved by a joint probability density function approach that utilizes higher-order moments of thermodynamic and dynamic variables. This study examines how well shallow cumulus and stratocumulus clouds are simulated by two versions of a CRM that is implemented with low-order and third-order turbulence closures (LOC and TOC) when a typical CRM horizontal resolution is used and what roles the subgrid-scale and resolved-scale processes play as the horizontal grid spacing of the CRM becomes finer.

Cumulus clouds were mostly produced through subgrid-scale transport processes while stratocumulus clouds were produced through both subgrid-scale and resolved-scale processes in the TOC version of the CRM when a typical CRM grid spacing is used. The LOC version of the CRM relied upon resolved-scale circulations to produce both cumulus and stratocumulus clouds, due to small subgrid-scale transports. The mean profiles of thermodynamic variables, cloud fraction and liquid water content exhibit significant differences between the two versions of the CRM, with the TOC results agreeing better with the LES than the LOC results. The characteristics, temporal evolution and mean profiles of shallow cumulus and stratocumulus clouds are weakly dependent upon the horizontal grid spacing used in the TOC CRM. However, the ratio of the subgrid-scale to resolved-scale fluxes becomes smaller as the horizontal grid spacing decreases. The subcloud-layer fluxes are mostly due to the resolved scales when a grid spacing less than or equal to 1 km is used. The overall results of the TOC simulations suggest that a 1-km grid spacing is a good choice

-

for CRM simulation of shallow cumulus and stratocumulus.

1. Introduction

Higher-order turbulence closure (HOC) and low-order turbulence closure (LOC) schemes, where closure assumptions are made on different orders of correlation terms, are extensively used to simulate boundary-layer turbulence and clouds. The recently-developed third-order closure (TOC) schemes, which are a subset of HOC schemes, have shown a strong ability to simulate stratocumulus, shallow cumulus and shallow cumulus-to-stratocumulus transition clouds (e.g., Golaz et al. 2002b; Lappen and Randall 2001b; Cheng and Xu 2006). The LOC schemes such as the K-theory and prognostic turbulence kinetic energy (TKE) schemes can also simulate these clouds rather well, but only if the counter-gradient transport of scalars and/or subgrid-scale condensation are appropriately represented (e.g., Wang 1993; Bechtold et al. 1995; Lock et al. 2000; Grenier and Bretherton 2001). This transport can be parameterized by using a modified K-theory or by combining with a mass flux scheme. Betchtold et al. (1995) related the variances of thermodynamic variables to their vertical gradients to obtain subgrid-scale condensation, based upon a statistical cloud scheme (e.g., Sommeria and Deardorff 1977; Mellor 1977).

The HOC schemes have traditionally been based on the assumption that a somewhat inaccurate approximation for the higher-order correlation terms will predict the lower–order moments adequately well (Lumley and Khajeh-Nouri 1974; André et al. 1976; Bougeault 1981a, b; Krueger 1988). However, Cheng et al. (2004) recently argued that a physically consistent formulation of third-order moments is important for the simulation of shallow cumulus clouds since the traditional quasi-Gaussian-based closure fails to simulate this and other boundary-layer cloud types (e.g., Krueger and Bergeron 1994). The recently developed TOC models predict the first, second and selected third order moments, which can be used to

determine the probability distribution function (pdf) for describing subgrid-scale distributions of various thermodynamic and dynamic properties (Lappen and Randall 2001a; Golaz et al. 2002a; Larson and Golaz 2005; Cheng and Xu 2006). Thus, this approach provides a physically consistent treatment for all moments. However, there are still difficulties in parameterizing the buoyancy production terms of the higher-order moment equations and the dissipation, as well as the pressure redistribution effects on the higher- and lower-order moments (Lappen and Randall 2006).

There are two types of LOC schemes. The first type is designed specifically for large-eddy simulations (LESs) (Smagorinsky 1963; Deardorff 1980), but is also extensively used in cloud-resolving models (CRMs) (e.g., Khairoutdinov and Randall 2003; Petch 2006). The horizontal grid spacings used in LESs range from a few meters to 100 meters, but those in CRMs usually exceed 1 km. The forms of parameterizations used in LESs and CRMs are identical except for the specifications of mixing length, which typically varies with grid size (e.g., Cuxart et al. 2000). Petch (2006) identified a 200 m horizontal grid size to be the maximum grid size to adequately simulate the transition from shallow to deep convection. There are no other studies that examine the validity of LOC schemes in CRM simulations of boundary-layer clouds. The second type of LOC schemes, which were developed and improved with LES results, do not only need to be combined with the mass flux scheme to properly simulate shallow cumulus clouds (e.g., Grenier and Bretherton 2001; Bretherton et al. 2004), but also need to incorporate alternative schemes in order to simulate stratocumulus clouds (e.g., Lock et al. 2000) or subgrid-scale condensation schemes (Bechtold et al. 1995).

Comparisons of the HOC and LOC schemes in simulations of boundary-layer clouds with grid spacings between those typically used in LESs and CRMs are difficult and rarely

performed. One of the reasons is that the effect of subgrid-scale condensation, which is typically negligible in the LOC scheme used in LESs, becomes more important as the grid spacing increases. This effect cannot be adequately formulated with the low-order moments unless the variances of thermodynamic variables are parameterized in terms of their vertical gradients (Bechtold et al. 1995). On the other hand, an HOC scheme uses the subgrid-scale condensation scheme to calculate the liquid water content and cloud fraction (e.g., Bougeault 1981a, b; Lappen and Randall 2001a; Golaz et al. 2002a). The cloud fraction and condensation depend on the joint pdf of the thermodynamic properties previously mentioned. A proper pdf with nonzero skewness can produce reasonable profiles of cloud fraction and liquid water content of shallow cumulus (Bougeault 1981a, b; Golaz et al. 2002b; Cheng and Xu 2006). Another reason for the difficulty is that the LOC and HOC schemes are not implemented in the same CRM. Most existing CRMs use either the LOC or the HOC schemes [see Xu et al. (2002)]. The HOC schemes are mostly implemented in a single-column model (SCM) framework or as ensemble-average models (e.g., Bougeault 1981b; Lappen and Randall 2001a; Golaz et al. 2002a), which parameterize the effects of turbulence and clouds and neglect the horizontal variability of turbulence.

The recently proposed MMF (Multi-scale Modeling Framework; Randall et al. 2003) approach, which uses a two-dimensional CRM to replace all cloud and turbulence parameterizations at every grid point of a conventional general circulation model (GCM), provides a good venue to further improve turbulence closure in the embedded CRM because all cloud regimes over the globe must be simulated by the CRM. The embedded CRM uses a horizontal grid size of 1-4 km. This grid spacing is too large to resolve any turbulence variability although stratocumulus clouds are simulated near the west coasts of the continents

where subsidence prevails (Khairoutdinov et al. 2005). The CRM in this MMF includes a $1\frac{1}{2}$-order turbulence closure (Khairoutdinov and Randall 2003). The LOC does not parameterize subgrid-scale condensation so that cloud condensation occurs only at the CRM grid scale. In particular, shallow cumulus clouds are not realistically represented by the large grid-spacing CRM. The seasonal-mean cloud fraction results from averaging the binary (0 or 1) cloud amount over all CRM grid cells within a grid point of the parent GCM.

The overarching goal of this study is to improve the simulation of boundary-layer clouds in the MMF. This may be achieved by implementing a TOC scheme in the CRM that is used for the MMF and then comparing the simulated results with those obtained using the same CRM with an LOC scheme. In the present study, we will examine how well shallow cumulus and stratocumulus are simulated by two versions of the CRM when the CRM grid resolution is coarse (as used in an MMF) but its vertical resolution is still high (compared to an MMF) and what roles the subgrid-scale and resolved-scale processes play as the horizontal grid spacing of the CRM increases from 250 m to 4 km. The second objective will be important for selecting appropriate grid spacings for a future MMF that implements an improved CRM, global cloud-resolving models (Miura et al. 2005) and cloud-resolving regional numerical weather prediction models. These two objectives are achieved by comparing CRM simulations with the LOC and TOC schemes against LES simulations for a few field experiment cases.

It is expected that there are significant differences in the simulated cloud and turbulence characteristics when the LOC and TOC schemes are used in the same CRM, due to the vastly different representations of subgrid-scale processes between the LOC and TOC schemes. We are not aware of a similar study that compares CRM simulations with HOC and

LOC schemes implemented in the same CRM, although intercomparison studies have compared simulations among CRMs with different types of turbulence closures (e.g., Xu et al. 2002, 2005; Grabowski et al. 2006) and SCM intercomparison studies of boundary-layer clouds have revealed some differences between the LOC and HOC schemes (Bechtold et al. 1996; Zhu et al. 2006). In the context of improving the CRM component of the MMF, this is a unique investigation.

Three diverse boundary-layer cloud cases are simulated by two versions of the CRM in this study. They are the BOMEX (Barbados Oceanographic and Meteorological Experiment, a marine shallow cumulus case; Siebesma et al. 2003), the ATEX (Atlantic Trade Wind Experiment, a broken stratocumulus case; Stevens et al. 2001), and the ASTEX (Atlantic Stratocumulus Transition Experiment, a stratocumulus case).

Section 2 introduces the CRM, the LOC and the TOC schemes. Section 3 describes the experiment design. The results from the two versions of the CRM are compared with those from LES in section 4. Summary and conclusions are presented in section 5.

2. Model description

A full description of the System for Atmospheric Modeling (SAM) CRM can be found in Khairoutdinov and Randall (2003). This CRM is embedded in an MMF (Khairoutdinov and Randall 2001). The model uses a fully staggered Arakawa C-type grid for the finite-difference representation of the anelastic model equations. The advection of momentum is computed with second-order finite differences in the flux form with kinetic energy conservation. The advection of scalars is monotonic with non-oscillatory options. One-moment bulk microphysics scheme of Kessler (1969) is used in SAM for liquid-phase clouds. Ice cloud microphysics and radiation schemes are not used in this study.

SAM includes a typical $1\frac{1}{2}$-order closure scheme, which predicts TKE and parameterizes the subgrid-scale vertical transports by turbulence but neglects the horizontal variability of turbulence. That is, except for minor differences in the values of the constants to calculate the subgrid-scale mixing length, which varies with grid size, the $1\frac{1}{2}$-order closure scheme is the same as Deardorff (1980) in principle. It does not include either a subgrid-scale condensation parameterization or a representation of counter-gradient transport of scalars. In this study, this scheme was not improved with these two missing aspects of LOC schemes mainly because improvement on specific elements of the LOC scheme is not the goal of this study and the embedded CRM in an MMF did not include them (Khairoutdinov and Randall 2001). It should be noted that both counter-gradient transport and subgrid-scale condensation by turbulence are parameterized in the TOC scheme to be described below.

A TOC scheme, which is called intermediately-prognostic higher-order closure (IPHOC), was implemented in SAM for this study in order to improve the simulation of boundary-layer clouds. Details of this closure can be found in Cheng and Xu (2006). The IPHOC assumes a joint double-Gaussian distribution of liquid-water potential temperature (θ_l), total water mixing ratio (q_t) and vertical velocity (w) [Mellor (1977); Larson et al. (2002)]. The distribution is inferred from the first, second, and third order moments of these variables, and is used to diagnose cloud fraction and grid-mean liquid water content, as well as the buoyancy term and fourth-order terms in the equations describing the evolution of the second- and third-order moments. The three most important third-order quantities, $\overline{\theta_l''^3}$, $\overline{q_t''^3}$ and $\overline{w''^3}$, along with all first- and second-order moments, are predicted explicitly, which gives the scheme its name (Intermediately Prognostic, IP).

The horizontal variability of turbulence is included in the IPHOC version of the CRM as in Krueger (1988), which differs from the HOC/LOC schemes used in ensemble-average or single-column models. The mixing length is calculated with a parcel method (Golaz et al. 2002a). The computational cost of the IPHOC model is about half of that of the fully prognostic TOC model (Krueger 1988), which predicts all third-order moments. The SAM CRM with IPHOC is about 25% more expensive than the standard SAM CRM. The IPHOC scheme has been tested in the University of California at Los Angeles-Langley Research Center CRM, where it has improved the simulation of shallow cumulus clouds and produces a gradual transition from shallow to deep convection (Cheng and Xu 2006).

3. Experiment design

The control experiments for all three cases use the LES version of SAM with a horizontal domain of 6.4 km x 6.4 km, a horizontal grid spacing of 100 m and a vertical grid spacing of 40 m. The exception is the ASTEX case, in which a smaller vertical grid spacing of 25 m is used to better resolve the shallow inversion layer above the top of the stratocumulus clouds. These simulations are treated as benchmarks for comparing the performance of the LOC and IPHOC versions of the CRM because the results of SAM LES boundary-layer cloud simulations are close to the consensus of LES inter-comparison studies (Moeng et al. 1996; Stevens et al. 2001; Siebesma et al. 2003).

We also performed a series of 2-D CRM simulations with the LOC and the IPHOC schemes for each case by only varying the horizontal grid spacing, but using a fixed horizontal domain of 256 km (x direction) and the LES vertical resolution described above. The largest horizontal grid spacing is 4 km, which is the largest CRM grid spacing used in an MMF (Khairoutdinov and Randall 2001). A 1-km grid spacing has also been used in an

MMF (Marchand, 2007; personal communication). The grid spacing of the finer-resolution simulation is halved from the next coarser-resolution simulation. The four other grid spacings used in the series of the simulations are 2 km, 1 km, 500 m and 250 m. The smallest grid spacing (250 m) is still much larger than that used in the LES, but it can partially resolve cumulus-scale circulations. A list of the experiments described above is given in Table 1. It is noted that diffusion coefficients in the momentum equations of SAM were different for grid spacings of 1 km or greater (CRM version) and less than 1 km (LES version). This switch in diffusion coefficients causes some changes in the temporal evolution of simulated clouds. Additional information on the configurations of each case will be described in section 4. For simplicity, we refer the CRM with the IPHOC scheme to as the IPHOC, and the CRM with the LOC scheme to as the LOC in the rest of this paper.

4. Results

In this section, results from three boundary-layer cloud cases will be presented, with emphases on the simulated cloud profiles, vertical transports and mean thermodynamic structures. More detailed results will be shown for the BOMEX case and for the resolution dependency of the IPHOC simulations because the differences between the LOC and IPHOC simulations in the other two cases are largely similar to those in the BOMEX case.

a. Shallow cumulus – the BOMEX case

Shallow cumuli exist in many regions of the tropical and subtropical oceans (e.g. Norris 1998; Xu et al. 2007) and continental regions with large vertical fluxes of sensible and latent heat. Convective transports by these clouds provide a source of moisture for the development of deep convective clouds in the tropics. Shallow cumulus clouds in the continental regions develop in the morning after sunrise when the sensible and latent heat

fluxes increase due to the solar heating. Shallow cumuli help to release the convective available potential energy (CAPE) gradually and prevent sudden development of deep convective clouds. A realistic simulation of shallow cumulus clouds is thus important for the representation of diurnal cycle of the convective processes in GCMs (Guichard et al. 2004; Grabowski et al. 2006).

BOMEX took place in the Caribbean region between 22 and 30 June 1969. It is a purely shallow cumulus case, no debris of stratocumulus clouds or mesoscale circulations were involved. Surface fluxes, large-scale subsidence and cloudtop radiative cooling are all prescribed in order to simulate a quasi-steady state, following the configuration designed by the GEWEX (Global Energy and Water-cycle Experiment) Cloud System Study (GCSS) boundary-layer cloud working group. Since the sizes of individual clouds are less than 1 km, the CRM simulations are not expected to resolve the shallow cumuli for the specified grid spacings except perhaps for the 250-m grid spacing. A detailed description of this case and results from LESs and observations can be found in Siebesma et al. (2003).

1) Cloud evolution and vertical fluxes

The simulated spatial distributions of clouds within the 2-D domain are fundamentally different between the LOC and IPHOC simulations. Partially cloudy grids with a grid cloud amount of less than 10% are evenly distributed within the CRM domain in the IPHOC simulation while a few percent of grids are cloudy and have large cloud water contents that are produced by resolved-scale circulations in the LOC simulation (not shown), due to the lack of a subgrid-scale condensation scheme in the LOC.

The evolution of cloud fraction from the IPHOC is shown in Fig. 1. All simulations were run for 6 h, although the 2- and 4-km grid-spacing LOC simulations need a longer

integration to achieve a steady state (Figs. 2a, b). The cloud base and top are located at approximately 500 m and 1500 m in all IPHOC simulations, respectively. The largest cloud fraction is at the bottom part of the cloud layer and decreases gradually towards cloud top. This is because most of the thinnest clouds were located at the low part of the cloud layer and they did not grow very high, due to the large entrainment associated with these clouds. The cloud fraction is less than 10% most of the time. These are the typical characteristics of the BOMEX shallow cumulus clouds simulated by LESs (Jiang and Cotton 2000; Siebesma et al. 2003). These results are generally independent of the horizontal grid spacing except that short-term fluctuations over the cloud layer increase as the grid spacing decreases. This suggests that the influence of resolved-scale circulations increases as the grid size decreases, because these circulations are better resolved in the finer grid-spacing simulations. The temporal fluctuations probably indicate that life cycles of a few simulated cumulus clouds within the 2-D domain may be coherent. This feature also appears in the LES results (Fig. 1f).

The LOC simulations also reproduce the general characteristics of the BOMEX cloud fractions, particularly, in the fine grid-spacing (0.25 – 1 km) simulations. As in the IPHOC simulations, the LOC solutions, where cloud fraction is determined from averaging of binary cloud amount, converge to that of the 3-D LES as the horizontal resolution increases (Fig. 2). There are, however, three major differences between the LOC and IPHOC simulations. First, the evolution of cloud fraction from the LOC depends greatly upon the horizontal resolution. For example, the highest clouds extend to 2000 m for the 4-km and 2-km grid-spacing simulations, 1800 m for the 1-km grid-spacing simulation, and 1600 m for the 500-m grid-spacing simulation, respectively. All of them are higher than the height of 1500 m simulated

by the LES. Secondly, the life cycle of each cloud event is long in the large grid-spacing simulations, e.g., 2-3 hours for the 4-km grid-spacing simulation. Third, the maximum cloud fractions for the large grid-spacing simulations are larger than those of the small grid-spacing simulations. These features are related to the inability of the LOC to deal with the skewed turbulence structure commonly observed in the cloud field and the slow response of resolved-scale circulations to the grid-scale instability created by the deficiency of the LOC scheme (Fig. 3b). It can be expected that the deficiency is less pronounced at the high-resolution simulations because the skewed turbulence structures can be marginally resolved. The grid-scale instability, however, does not vary much with time in any of the IPHOC simulations and is similar to that of the LES (Fig. 3a). This is because the deficiencies of the IPHOC are not as pronounced as those in the LOC, due to the pdf representation of subgrid-scale circulations and related condensation.

The transition from the smooth to highly-fluctuating evolution in cloud fraction seen from Figs. 1a-e suggests that there is a change in the partitioning of resolved-scale and subgrid-scale transports as the grid spacing changes (Fig. 4). The profiles of subgrid-scale ($\overline{w''\theta_l''}$ and $\overline{w''q_t''}$) and resolved-scale ($\overline{w'\theta_l'}$, $\overline{w'q_t'}$) transports of θ_l and q_t are shown in Fig. 4, and are averaged over the last three hours of the IPHOC simulations so that the initial spinup period is excluded. Here, the subgrid scale fluxes are produced from the turbulence parameterization while the resolved-scale fluxes are directly diagnosed from resolved-scale variables. Note that the LES fluxes are plotted along with the subgrid-scale fluxes from the IPHOC. The LES shows a nearly parabolic profile of $\overline{w''\theta_l''}$ between 0 and 2 km with a minimum of -20 W m^{-2} at 0.9 km and a monotonically-decreasing profile of $\overline{w''q_t''}$ from 155 W m^{-2} at the surface to 0 W m^{-2} at 2 km.

The profiles of $\overline{w"\theta_l"}$, $\overline{w"q_t"}$, $\overline{w'\theta_l'}$ and $\overline{w'q_t'}$ from the IPHOC simulations vary systematically with the grid spacing. The magnitudes of $\overline{w"\theta_l"}$ and $\overline{w"q_t"}$ increase as the grid spacing increases while the magnitudes of $\overline{w'\theta_l'}$ and $\overline{w'q_t'}$ decrease as the grid spacing increases. In particular, the total fluxes, which is the sum of the subgrid-scale and resolved-scale fluxes, are solely determined by the subgrid-scale fluxes in the 4-km grid-spacing simulation while they are mostly determined by the resolved-scale fluxes in the 250-m grid-spacing simulation except for the near-surface layer. This is an expected result because a subgrid-scale parameterization should play a more significant role in the coarse-resolution simulations than in the fine-resolution simulations.

Another interesting result is how the vertical profiles of these fluxes change as the grid spacing increases. A two-layer structure, i.e., the subcloud and cloud layers, is easily identified in the flux profiles of the high-resolution simulations (Fig. 4). The subcloud layer being located at above the surface layer and below the cloud base (500 m) is driven by thermal circulations. These circulations are mostly resolved by the 250-m and 500-m grid-spacing simulations but only partially simulated by the 1-km and 2-km grid-spacing simulations. At the lowest 0.2 km, i.e., the lowest portion of the subcloud layer or the near-surface layer, the subgrid-scale fluxes are significant at the high-resolution simulations. This is also well captured by all LOC simulations (not shown). That is, $\overline{w"\theta_l"}$ and $\overline{w"q_t"}$ from the LOC simulations are nearly zero for the layer above 0.2 km (similar to the 250-m IPHOC run shown in Fig. 4) and show little dependency on the grid spacing. The profiles of the resolved-scale fluxes resemble the profiles produced from the LES, except for the larger magnitudes in the cloud layer (not shown) due to the overestimated cloud top heights in the LOC simulations (Figs. 2a-e). Therefore, the resolved-scale transports compensate for the lack of

subgrid-scale vertical transports in all LOC simulations, which are due to the deficiencies in the LOC scheme discussed earlier.

2) Mean thermodynamic profiles

This section describes the mean vertical structures of thermodynamic variables in relation to the simulated characteristics of shallow cumulus discussed earlier. Shallow cumulus clouds have a three-layer thermodynamic structure: a well-mixed subcloud layer, a conditionally unstable cloud layer, and a weak inversion layer above cloud top. These structures are well simulated by the LES and IPHOC, as seen from the θ_l and q_t profiles (Figs. 5a, b). This result can be explained by the convergences of the total fluxes, the vertical shapes of which are generally similar between the LES and IPHOC simulations (not shown).

Although the θ_l and q_t profiles of all five IPHOC simulations are close to LES, the profiles of the high-resolution simulations deviate slight more from the LES than those of the coarse-resolution simulations except for the subcloud layer. That is, the cloud layer is slightly drier and warmer and the layer above the weak inversion is more moist and cooler in the high-resolution simulations. This result may be explained by the fact that cumulus circulations in the 250-m and 500-m grid-spacing simulations are marginally resolved and in two dimensions, compared to the 3-D nature of the LES. When the grid spacing is coarse, the turbulent transports that may capture the collective effects of 3-D circulations are more active and thus better able to reproduce the thermodynamic structures.

The impact of 2-D resolved-scale circulations on the thermodynamic structures can be further seen from a comparison with the LOC results (Figs. 6a, b). The 1-km grid-spacing LOC and IPHOC simulations are chosen for this purpose. As discussed earlier, the turbulent transports in the LOC are very weak. So the 2-D resolved-scale flows produce artificially

strong transports to substitute for the lack of subgrid-scale transports. Thus, the thermodynamic structures of the LOC simulation deviate more greatly from those of the LES than the IPHOC simulation, due to the lack of turbulent transports in the cloud layer that are artificially replaced by the resolved-scale transports, whose vertical gradients are relatively weak within the low and middle portions of the cloud layer but very strong at the top portion (not shown). The lack of turbulent transports can be relieved somewhat by implementing an alternative dissipation length-scale formulation in the LOC, which may include more complicated physics, such as that proposed by Blackadar (1962). Tests with the Blackadar (1962) formulation showed that the subgrid-scale transports in the subcloud-layer increased, but those in cloud layer were about the same as before for this case but increased in the ASTEX case (with a strong inversion). An empirical subgrid-scale condensation (e.g., Bechtold et al. 1995) may also be needed to further improve the LOC simulations.

As shown in Fig. 1, the temporal evolutions of cloud fraction differ among the IPHOC simulations with different horizontal grid spacings. The steady state in the 4-km grid-spacing simulation is not reached until 10 h (not shown). To a lesser extent, this is also true in the 2-km grid-spacing simulation. Because of this, the mean cloud fractions averaged over the last three hours of these two simulations are slightly higher than the LES and the high-resolution simulations (Fig. 5d). On the other hand, the liquid water contents in the upper cloud layer of these simulations are lower than those of the higher-resolution simulations (Fig. 5c). The differences from LES do not systematically vary with grid spacing. And the difference is less than 50% between any pair of simulations, which is much smaller than the 10-fold difference in liquid water path among SCMs with different turbulence closures (Zhu et al. 2005). This suggests that it is difficult to simulate the liquid water content even when θ_l

and q_t profiles are very similar between simulations (Figs. 5a, b). Compared to the differences between the LOC and IPHOC 1-km grid-spacing simulations (Figs. 6c, d), the differences among the IPHOC simulations are not significant.

b. Stratocumulus – the ASTEX case

Stratocumulus clouds are very important for the Earth's radiation budget. They have higher cloud fractions than shallow cumulus clouds, with cloud top temperatures close to that of the Earth's surface. They have a relatively minor effect on the longwave radiation emitted to space, but can increase the Earth's albedo. Studies have shown that slight changes of their cloud amount, liquid water content or cloud droplet radius can significantly change the global radiation budget (e.g., Ramanathan et al. 1989; Slingo 1990). Stratocumulus clouds are formed in the subsidence regions of the Hadley cell. Typically, the inversion above the cloud top is stronger and sea surface temperature is lower for stratocumulus clouds than for shallow cumulus clouds (e.g., Xu et al. 2007).

ASTEX took place over the area near the Azores and Madeira Islands in the Atlantic Ocean off North Africa on 1-28 June 1992 (Albrecht et al. 1995). A stratocumulus case with no drizzle was configured based upon the ASTEX observations (Roode and Duynkerke 1997)[1], which represent a typical stratocumulus-topped boundary layer. The simulation of this case lasts for 3 h, beginning at 0400 UTC 13 June 1992. The cloud deck has a thickness of 400 m, extending from 300 m to 700 m. The temperature jump is 5.5 K at the inversion. The simulations are initiated with an adiabatic cloud liquid water profile, with a peak value of ~0.7 g kg^{-1}, and prescribed with surface sensible and latent heat fluxes. A simple,

[1] Details of the configuration can be found in http://www.phys.uu.nl/~roode/ASTEX.html.

interactive radiation scheme is included; the radiative flux is diagnosed from the predicted liquid water content, but there is no clearsky cooling.

The overall evolution of cloud fraction is similar among the LOC, IPHOC and LES simulations in the sense that the overcast cloud deck between 300 and 700 m is well simulated. Minor differences can be noticed at the bottom of cloud layer and the top of cloud layer, however (Fig. 7). Since the simulated cloud characteristics are not greatly dependent upon the grid spacing, only the 1-km grid-spacing LOC and IPHOC simulations are shown in Figs. 7b, c. The cloud bases in the IPHOC simulation and the cloud tops in the LOC simulations are somewhat lower than the LES (Fig. 7a) although they are within the uncertainties of measurements. This result can be seen from the averaged profiles over the last two hours of the IPHOC simulations (Fig. 8d). The LOC results for this case will not be described below because the discrepancies in the resolved-scale and turbulent flux profiles are similar to those noted earlier while the mean thermodynamic profiles are largely similar to those simulated by the IPHOC.

The differences in the θ_l and q_t profiles between the IPHOC and LES (Figs. 8a, b) are due mainly to those in the total transports (Fig. 9) because the radiative cooling and large-scale subsidence are nearly identical (not shown). As in the BOMEX cumulus case, most transports are determined by the subgrid scales for the 1-, 2- and 4-km grid-spacing simulations but determined by the resolved scales for the 250- and 500-m grid-spacing simulations. Since this is a stratocumulus-topped boundary-layer case, the stratocumulus clouds are parts of the boundary layer. The size of eddies determines whether or not the resolved scales are the dominant player in the boundary-layer circulations. These eddies can be marginally resolved in the 250- and 500-m grid-spacing simulations. This explains why

the resolved-scale fluxes in the cloud layer are relatively larger for these two simulations (Figs. 9b, d). Due to the fact that the subcloud layer is a part of the stratocumulus-topped boundary layer, the resolved-scale fluxes there are very small. This feature is present for all IPHOC simulations. This is a major distinction from the BOMEX case.

The gradient of q_t at the top part of cloud layer (Fig. 8b) is largely maintained through the resolved-scale transport of q_t for the 250- and 500-m grid-spacing simulations. For coarse-resolution simulations, the gradient of q_t is not maintained because the subgrid-scale fluxes are underestimated for the three simulations in question. This result agrees with Zhu et al. (2005). They showed that some SCMs tend to smooth the sharp jumps of θ_l and q_t a little at the cloud top and have larger gradients in θ_l and q_t within the mixed layer. They suspected that the SCM inversion structure depends on details of its turbulent parameterization.

Because the sharp q_t inversion of the ASTEX stratocumulus is not captured in the three coarse-resolution simulations, the maximum liquid water content was underestimated by the IPHOC (Fig. 8c). There are false positive $\overline{w"\theta_l"}$ fluxes in the layer above cloud top that were produced by the turbulence closure (Fig. 9a) despite the fact that the negative peak at the top of the cloud layer is well produced. This result is consistent with the lack of sharp peaks in the variance and skewness of θ_l and q_t within this thin layer produced by the IPHOC closure (not shown). This inherent difficulty also appears in the simulations of Golaz et al. (2002b), in which the IPHOC turbulence closure shares the double-Gaussian pdf description of subgrid-scale properties.

c. Broken stratocumulus – the ATEX case

ATEX took place in the northwest tradewind region of the Atlantic in February 1969, where clouds there were in the transition from shallow cumulus to stratocumulus, or broken

stratocumulus. The observations were based on three ships that drifted for about three weeks in this region, with intensive observations being concentrated in the lowest 4 km of the atmosphere (e.g., Augstein et al. 1973). The LES inter-comparison study of this case found that the cloud amount is sensitive to the numerical algorithms among the participating models (Stevens et al. 2001). The configuration for this intercomparison case is followed in the present study. Specifically, both radiation and surface fluxes are interactive. The sea surface temperature is prescribed to be 298 K. An exception to the intercomparison configuration is that the simulated domain-averaged wind profile is nudged to its initial profile with a nudging time scale of 4 h (Xu and Randall 1996). This helps to minimize the differences in the calculated surface turbulent fluxes between simulations.

As in the BOMEX case, simulated cloud spatial distributions and resolved-scale circulations within the 2-D domain are quite different between the LOC and IPHOC simulations (not shown). For a given grid spacing, the resolved-scale circulations simulated by both versions of the CRM are, as shown later, much stronger than those in the BOMEX case due to stronger interactive radiative cooling at the cloud top. This is one of the fundamental differences between the BOMEX and ATEX cases.

The LES-simulated cloud fraction of the ATEX case exhibits characteristics of both shallow cumulus and stratocumulus clouds (Fig. 10f). There are two maximum centers of cloud fraction at the bottom and top parts of the cloud layer. The cloud fraction in the bottom part of the cloud layer is less than 10%, which is mostly due to shallow cumulus clouds. Surface sensible and latent heat fluxes provide convective buoyancy for air parcels near the surface. When these positively-buoyant air parcels reached the lifting condensation level, shallow cumuli were produced. The cloud fraction near the cloud top is about 40%, which is

mainly composed of stratocumulus clouds. The minimum in cloud fraction in the middle of the cloud layer is likely caused by cloud-top entrainment instability (CTEI; Randall 1980; Stevens et al. 2001), i.e., mixing of cloud-top air with warm and dry air can lead to negative buoyancies of mixed parcels, which sink to the middle of the cloud layer.

The IPHOC simulation reproduced both the stratocumulus (~30-40% at the top part of cloud layer) and shallow cumulus maxima (~5-10%), but only for the first half of the 8-h integration with the 1-, 2- and 4-km grid spacings (Figs. 10a-c) and the entire integration period with the 250- and 500-m grid spacings (Figs. 10d, e). Note that the 4-km grid-spacing simulation did not achieve a quasi-steady state until 14 h (not shown) and the steady state was not reached within 8 h in the 2-km grid-spacing simulations, either. The cloud fraction minimum in the middle of the cloud layer for the quasi-steady state was not reproduced well when the grid spacing was larger than 1 km, due presumably to the weak cloud-top entrainment.

The LOC simulations produced slightly higher cloud bases and larger cloud amounts than the 3D-LES and IPHOC simulations, especially when grid spacings are large. The onset of shallow cumulus and stratocumulus clouds was delayed more as the horizontal grid spacing increased (Figs. 11a-e). The mechanism for this delay is similar to that described for the BOMEX cumulus case, i.e., due to the inability of the LOC scheme to deal with the skewed turbulence structure within cloud field. In the LOC simulations, cumulus clouds are produced by resolved-scale circulations, which need more time at the larger horizontal grid spacings to build up sufficient CAPE (see Fig. 3a). In the IPHOC, on the other hand, cumulus clouds are produced by subgrid-scale turbulence. In nature, interaction with radiation drives both resolved-scale and subgrid-scale circulations at the top part of cloud layer, which

produces the stratocumulus maximum. In the LOC simulations, stratocumulus clouds appear well after shallow cumuli have occurred, which suggests that the stratocumulus clouds are initially produced by the resolved-scale circulations, rather than radiatively-driven turbulence.

There are two major similarities between the ATEX and BOMEX cases regarding the grid-scale and subgrid-scale fluxes (Figs. 4 and 12). First, the magnitudes of $\overline{w"\theta_l"}$ and $\overline{w"q_t"}$ increase as the grid spacing increases while the magnitudes of $\overline{w'\theta_l'}$ and $\overline{w'q_t'}$ decrease as the grid spacing increases. An exception is that the 250-m grid-spacing simulation has larger magnitudes of $\overline{w"\theta_l"}$ and $\overline{w"q_t"}$ near the cloudtop layer than those of 500-m and 1-km grid-spacing simulations. Second, the subcloud-layer fluxes are dominated by those of the resolved scales for all IPHOC simulations except for the 4-km grid-spacing simulation. For example, the subcloud-layer $\overline{w'q_t'}$ is identical for 250-m, 500-m and 1-km grid-spacing simulations. The most significant difference between the ATEX and BOMEX cases is that subgrid-scale fluxes ($\overline{w"\theta_l"}$ and $\overline{w"q_t"}$) have small contributions to the total transports within the cloud layer of the ATEX case (Fig. 12). This is due to the presence of stratocumulus clouds in the ATEX case, which are less convective than shallow cumulus clouds and better resolved by the CRM simulations.

For the ATEX case, the inversion at the cloud top (Fig. 13a, b) is stronger than in the BOMEX case, but weaker than in the ASTEX case. The unstable layer and the well-mixed layer can still be distinguished from the mean profiles of θ_l and q_t produced by the IPHOC and LES, but the mixed layer in the q_t profile of the LOC 1-km grid-spacing simulation deviates more from the LES than the corresponding IPHOC simulation. This may be due to the different vertical structures of $\overline{w'q_t'}$ simulated by the LOC (not shown). This is also

related to the unrealistically large amount of stratocumulus clouds and liquid water content (Figs. 13c, d), e.g., by a factor of 2 near the cloud top for liquid water content.

The overestimates of both cloud fraction and liquid water content are small for the IPHOC simulations, compared to the LOC simulations (Figs. 13c, d) although they depend systematically upon the grid spacing (not shown), unlike those shown for the BOMEX case (Fig. 5). In particular, the overestimates appear in the middle of the cloud layer, with the largest differences for the 2- and 4-km grid-spacing simulations. The overestimates for the 250- and 500-m grid-spacing simulations are similar to those of the 1-km grid-spacing simulation (Figs. 13c, d). In combining with the flux profiles shown in Fig. 12, which shows almost no difference in the subcloud-layer fluxes among the 250-m, 500-m and 1-km grid-spacing simulations, one may argue that the 1-km grid spacing is a good choice for the coarsest "acceptable" resolution. A similar argument can be made for the BOMEX case, based upon all the parameters examined. This chosen grid spacing is larger than the 200 m identified by Petch (2006) using a CRM with a LOC. This suggests that the implementation of the TOC can allow for the use of a larger grid size for realistic CRM simulations of boundary-layer clouds than is possible for a CRM with the LOC.

5. Summary and conclusions

This study has examined whether shallow cumulus and stratocumulus clouds are adequately simulated by two versions of a CRM with low-order and third-order turbulence closures (LOC and TOC) when a typical CRM horizontal grid spacing is used and what roles the subgrid-scale and resolved-scale processes play as the horizontal grid spacing of the CRM increases. CRM simulations were performed in the 2D framework. The 2D framework is similar to that employed in the MMF with a domain size of 256 km, but different from that

employed in the MMF because horizontal grid spacings ranging from 250 m to 4 km and higher vertical resolutions were used. These simulations have been compared with benchmarks obtained from LES simulations. The major conclusion of this study is that the CRM with TOC performs reasonably well for all grid spacings between 250 m and 4 km although small grid spacings can better simulate subcloud-layer processes. The detailed findings can be summarized as follows.

The initiation and evolution of boundary-layer clouds in the two versions of the CRM are significantly different when typical CRM grid spacings are used. The LOC version of the CRM relied on the resolved-scale circulations to produce boundary-layer shallow cumulus clouds and the simulated clouds underwent large temporal fluctuations at coarse resolutions, due to a combination of factors: (i) the inability of the LOC to deal with skewed turbulence structures, (ii) the lack of subgrid-scale condensation, (iii) the lack of subgrid-scale transports in the upper part of the subcloud layer and the cloud layer, and (iv) the slow response of resolved-scale circulations to the grid-scale instability created by the deficiencies of the LOC scheme.

On the other hand, the IPHOC version of the CRM produced shallow cumulus clouds mainly through subgrid-scale processes, which underwent smooth evolutions at coarse resolutions. There was no delay in the initiation of shallow cumulus clouds, due to adequately formulated subgrid-scale transports. These differences in the cloud initiation and evolution between the two versions of the CRM also appeared in the broken stratocumulus case because models start without any cloud for both cases. The ASTEX stratocumulus case did not show such differences because clouds were initially specified. At high resolutions, as expected, the simulated cumulus and broken stratocumulus underwent similar evolutions for

both versions of the CRM. They showed high-frequency temporal variations and reasonably similar vertical structures, as in the LES, due to the increased amplitudes of resolved-scale transports and adequate simulations of subcloud-layer circulations. The differences are, however, still not negligible between the two versions of the CRM because subgrid-scale condensation is not produced.

Differences in the various characteristics of the quasi-steady states, including cloud properties, between the two versions of the CRM are more significant than those between the IPHOC simulations with different grid spacings. The results from the 1-km grid-spacing simulations with the two versions of the CRM were extensively compared to illustrate the differences between the CRMs. The relatively small differences between the IPHOC and LES depend upon the grid spacing used. In the cumulus and broken stratocumulus cases, the deviations of the θ_l and q_t profiles of the high-resolution simulations (250- and 500-m) from the LES profiles are slightly more pronounced, due to the fact that cumulus circulations are marginally resolved and in two dimensions. In coarse-resolution simulations, the collective effects of 3-D circulations are better captured by the parameterized turbulent transports. In the stratocumulus case, the opposite is true; i.e., the gradient of q_t is not well maintained for the coarse resolution simulations, due to the underestimates of subgrid-scale fluxes, as in other similar turbulence closures (e.g., Golaz et al. 2002b; Zhu et al. 2005). The resolved-scale transport in the cloud layer compensates for the underestimate of subgrid-scale fluxes in the high-resolution simulations.

For all three cases, the partitioning between the resolved-scale and subgrid-scale fluxes from the IPHOC is reasonable. The magnitudes of subgrid-scale fluxes increase as the grid spacing increases while the magnitudes of resolved-scale decrease as the grid spacing

increases. The total fluxes are solely due to the subgrid-scale fluxes for the coarsest resolution (4 km) simulation while they are mostly due to the resolved-scale fluxes for the highest resolution (250 m) simulation. At relatively high resolutions, the resolved scales are responsible for most transports within the subcloud layer of cumulus and broken stratocumulus clouds. This may be an important factor in choosing an acceptable resolution, along with the other characteristics of the simulations. A 1-km grid spacing can be a good choice, because a significant fraction of the total fluxes comes from the resolved scale in the subcloud layer while the parameterized fluxes in the cloud layer are reasonably large. This chosen grid spacing is larger than the 200 m identified by Petch (2006) using a CRM with a LOC. Thus, the incorporation of a TOC in a CRM allows for the use of a larger grid size than is possible for a CRM with a LOC although it increases computational costs at the same grid spacing, as mentioned in section 2. The net effect of using a larger grid spacing will, however, save computational costs. The choice of an appropriate vertical grid spacing has not been discussed in this study, which will be given in a future study.

As the computational power increases, MMFs and global CRMs will play an important role to address important climate issues. The difficulties in parameterization of deep convective clouds can be avoided in such models, but those in the parameterization of boundary-layer clouds remain. One can see the impacts of the different turbulence closure schemes on cloud evolution, resolved-scale circulation, vertical transport of θ_l and q_t and the mean thermodynamic profiles presented in this study. Many aspects of cloud evolution and thermodynamic structures from the IPHOC are comparable to the benchmark LES results. It will be interesting to study the impact of the IPHOC in a global model because there are

significant uncertainties in cloud feedbacks associated with boundary-layer clouds in traditional climate models (Bony and Defresne 2005).

Acknowledgments: This work was supported by Office of Biological and Environmental Research, U.S. Department of Energy as part of the Atmospheric Radiation Measurement (ARM) Program, under interagency agreement DE-AI-02-06ER64183 and by NASA Modeling, Analysis and Prediction Program (Dr. Don Anderson, program manager). The authors would like to thank Dr. Marat Khairoutdinov of Colorado State University for providing the SAM model codes used in this study. He is also thanked for providing invaluable advice for coupling the third-order closure with the SAM. Drs. Zachary Eitzen and Takmeng Wong are thanked for reading drafts of this paper.

References

Albrecht, B. A., C. S. Bretherton, D. Johnson, W. H. Schubert, A. S. Frisch, 1995: The Atlantic Stratocumulus Transition Experiment—ASTEX. *Bull. Amer. Meteor. Soc.,* **76**, 889-904.

André, J. C., G. De Moor, P. Lacarrère, and R. Du Vachat, 1976: Turbulence approximation for inhomogeneous flows. Part I: The clipping approximation. *J. Atmos. Sci.,* **33,** 476-481.

Augstein, E., H. Riehl, F. Ostapoff, and V. Wagner, 1973: Mass and energy transports in an undisturbed Atlantic trade-wind flow. *Mon. Wea. Rev.,* **101,** 101-111.

Bechtold, P., J. Cuijpers, P. Mascart, P. Trouihet, 1995: Modeling of trade wind cumuli with a low-order turbulence model: Toward a unified description of Cu and Sc clouds in meterological models. *J. Atmos. Sci.,* **52,** 455-463.

Bechtold, P., S. K. Krueger, W. S. Lewellen, E. van Meijgaard, C.-H. Moeng, D. A. Randall, A. van Ulden, and S. Wang, 1996: Modeling of a stratocumulus-topped PBL: Intercomparison among different one-dimensional codes and with large eddy simulation. *Bull. Amer. Meteor. Soc.,* **77,** 2033-2042.

Blackadar, A. K., 1962: The vertical distribution of wind and turbulent exchange in a neutral atmosphere. *J. Geophys. Res.*, **67,** 3095 3120.

Bony, S., and J.-L. Dufresne, 2005: Marine boundary layer clouds at the heart of tropical cloud feedback uncertainties in climate models. *Geophys. Res. Lett.,* **32,** L20806, doi:10.1029/2005GL023851.

Bougeault, P., 1981a: Modeling the trade-wind cumulus boundary layer. Part I: Testing the ensemble cloud relations against numerical data. *J. Atmos. Sci.,* **38,** 2424-2428.

Bougeault P., 1981b: Modeling the trade-wind cumulus boundary layer. Part II: A high-order one-dimensional model. *J. Atmos. Sci,* **38,** 2429–2439.

Bretherton, C. S., J. R. McCaa, and H. Grenier, 2004: A new parameterization for shallow cumulus convection and its application to marine subtropical cloud-topped boundary-layer. Part I: Description and 1D results. *Mon. Wea. Rev.,* **132,** 864-882.

Cheng, A. K.-M. Xu, and J.-C. Golaz, 2004: Liquid water osciilation in modeling boundary-layer cumuli with third-order turbulence closure models. *J. Atmos. Sci.,* **61,** 1621-1629.

Cheng A., and K.-M. Xu, 2006: Simulation of shallow cumuli and their transition to deep convective clouds by cloud-resolving models with different third-order turbulence closures. *Q. J. Roy. Meteor. Soc.* **132**, 359-382.

Cuxart, J. P. Bougeault, and J.-L. Redelsperger, 2000: A turbulence scheme allowing for mesoscale and large-eddy simulations. *Q. J. Roy. Meteor. Soc.,* **126,** 1-30.

Deardorff, J. W., 1980: Stratocumulus-capped mixed layers derived from a three-dimensional model. *Bound.-Layer Meteor.*, **18**, 495-527.

Golaz, J.-C., V. E. Larson, and W. R. Cotton, 2002a: A PDF based model for boundary layer clouds. Part I: Method and model description. *J. Atmos. Sci.,* **59,** 3540-3551.

Golaz, J.-C., V. E. Larson, and W. R. Cotton, 2002b: A PDF based model for boundary layer clouds. Part II: Model results. *J. Atmos. Sci.,* **59,** 3552-3571.

Grabowski, W. W., P. Bechtold, A. Cheng, R. Forbes, C. Halliwell, M. Khairoutdinov, S. Lang, T. Nasuno, J. Petch, W.-K. Tao, R. Wong, X. Wu, K.-M. Xu, 2006: Daytime convective development over land: A model intercomparison based on LBA observations. *Q. J. Roy. Meteor. Soc.,* **132,** 317-344.

Grenier, H., and C. S. Bretherton, 2001: Moist PBL parameterization for large-scale models and its application to subtropical cloud-topped marine boundary layers. *Mon. Wea. Rev.,* **129,** 357-377.

Guichard, F., J. C. Petch, J. L. Redelsperger, P. Bechtold, J. P. Chaboureau, S. Cheinet, W. W. Grabowski, H. Grenier, C. G. Jones, M. Kohler, J. M. Piriou, R. Tailleux, and M. Tomasini, 2004: Modelling the diurnal cycle of deep precipitating convection over land with cloud-resolving models and single-column models. *Q. J. Roy. Meteor. Soc.,* **130,** 3139-3172.

Jiang, H., and W. R. Cotton, 2000: Large eddy simulation of shallow cumulus convection during BOMEX: Sensitivity to microphysics and radiation. *J. Atmos. Sci.,* **57,** 582-594.

Kessler E. III, 1969: On the Distribution and Continuity of Water Substance in Atmospheric Circulation. *Meteor. Monogr.,* **32,** Amer. Meteor. Soc., 84 pp.

Khairoutdinov, M. F., and D. A. Randall, 2001: A cloud-resolving model as a cloud parameterization in the NCAR Community Climate System Model: Preliminary results. *Geophys. Res. Lett.* **28,** 3617-3620.

Khairoutdinov, M. F., and D. A. Randall, 2003: Cloud resolving modeling of the ARM summer 1997 IOP: Model formulation, results, uncertainties, and sensitivities. *J. Atmos. Sci.,* **60,** 607–625.

Khairoutdinov, M. F., D. A. Randall, and C. DeMott, 2005: Simulations of the atmospheric general circulation using a cloud-resolving model as a superparameterization of physical processes. *J. Atmos. Sci.,* **62,** 2136–2154.

Krueger, S. K., 1988: Numerical simulation of tropical cumulus clouds and their interaction

with the subcloud layer. *J. Atmos. Sci.,* **45,** 2221-2250.

Krueger, S. K., and A. Bergeron, 1994: Modeling the trade cumulus boundary layer. *Atmos. Res*, **33,** 169–192.

Lappen, C.-L., and D. A. Randall, 2001a: Toward a unified parameterization of the boundary layer and moist convection. Part I: A new type of mass-flux model. *J. Atmos. Sci.,* **58,** 2021-2036.

Lappen, C.-L., and D. A. Randall, 2001b: Toward a unified parameterization of the boundary layer and moist convection. Part III: Simulations of clear and cloudy convection. *J. Atmos. Sci.,* **58,** 2052-2072.

Lappen, C.-L., and D. A. Randall, 2006: Parameterization of pressure perturbations in a PBL mass-flux model. *J. Atmos. Sci.,* **63,** 1726–1751.

Larson, V. E., and J.-C. Golaz, 2005: Using probability density functions to derive consistent closure relationships among higher-order moments. *Mon. Wea. Rev.,* **133,** 1023-1042.

Larson, V. E., J.-C. Golaz, and W. R. Cotton, 2002: Small-scale and mesoscale variability in cloudy boundary layers: Joint probability density functions. *J. Atmos. Sci.,* **59,** 3519-3539.

Lock, A. P., A. R. Brown, M. R. Bush, G. M. Martin, and R. N. B. Smith, 2000: A new boundary layer mixing scheme. Part I: Scheme description and single-column model tests. *Mon. Wea. Rev.,* **128,** 3187-3199.

Lumley, J. L., and B. Khajeh-Nouri, 1974: Computational modeling of turbulent transport. *Adv. Geophy.,* **18A**, Academic Press, 169-192.

Mellor G. L., 1977: The Gaussian cloud model relations. *J. Atmos. Sci,* **34,** 356–358.

Miura, H., H. Tomita, T. Nasuno, S. Iga, M. Satoh, and T. Matsuno, 2005: A climate

sensitivity test using a global cloud resolving model under an aqua planet condition, *Geophys. Res. Lett.,* **32,** L19717, doi:10.1029/2005GL023672.

Moeng, C.-H., W. R. Cotton, C. S. Bretherton, A. Chlond, M. F. Khairoutdinov, S. K. Krueger, W. S. Lewellen, M. K. MacVean, J. R. M. Pasquier, H. A. Rand, A. P. Siebesma, B. Stevens, and R. I. Sykes, 1996: Simulation of a stratocumulus-topped planetary boundary layer: Intercomparison among different numerical codes. *Bull. Amer. Meteor. Soc.,* 77, 261-278.

Norris, J. R., 1998: Low cloud type over the ocean from surface observations: Part II: Geographic and seasonal variations. *J. Climate,* **11,** 383-403.

Petch, J. C., 2006: Sensitivity studies of developing convection in a cloud-resolving model. *Q. J. Roy. Meteor. Soc.,* **132,** 345-358.

Ramanatham, V., R. D. Cess, E. F. Harrison, P. Minnis, B. R. Barkstrom, E. Ahmad, and D. Hartmann, 1989: Cloud-radiative forcing and climate: Results from the Earth Radiation Budget Experiment. *Science,* **243**, 57-63.

Randall, D. A., 1980: Conditional instability of the 1st kind upside-down. *J. Atmos. Sci.,* **37,** 125-130.

Randall, D. A., M. F. Khairoutdinov, A. Arakawa, and W. W. Grabowski, 2003: Breaking the cloud parameterization deadlock. *Bull. Amer. Meteor. Soc.*, **84**. 1547–1564.

Roode, S. R. de and P. G. Duynkerke, 1997: Observed Lagrangian transition of stratocumulus into cumulus during ASTEX: Mean state and turbulence structure. *J. Atmos. Sci.*, **54,** 2157-2173.

Siebesma, A. P., C. S. Bretherton, A. Brown, A. Chlond, J. Cuxart, P. G. Duynkerke, H. Jiang, M. Khairoutdinov, D. C. Lewellen, C.-H. Moeng, E. Sanchez, B. Stevens, and

D. E. Stevens, 2003: A large eddy simulation intercomparison study of shallow cumulus convection. *J. Atmos. Sci.,* **60,** 1201-1219.

Slingo, A., 1990: Sensitivity of the Earth's radiation budget to changes in low clouds. *Nature*, **343**, 49-50.

Smagorinsky, J., 1963: General circulation experiments with the primitive equations: I. The basic experiment. *Mon. Wea. Rev.,* **91,** 99–164.

Sommeria G., and J. W. Deardorff, 1977: Subgrid-scale condensation in models of nonprecipitating clouds. *J. Atmos. Sci,* **34,** 344–355.

Stevens, B., A. S. Ackerman, B. A. Albrecht, A. R. Brown, A. Chlond, J. Cuxart, P. G. Duynkerke, D. C. Lewellen, M. K. Macvean, R. A. J. Neggers, E. Sanchez, A. P. Siebesma, and D. E. Stevens, 2001: Simulations of trade wind cumuli under a strong inversion. *J. Atmos. Sci.,* **58,** 1870-1891.

Wang, S., 1993: Modeling marine boundary-layer clouds with a two-layer model: a one-dimensional simulation. *J. Atmos. Sci.,* **50,** 4001–4021.

Xu, K.-M., and D. A. Randall, 1996: Explicit simulation of cumulus ensembles with the GATE Phase III data: Comparison with observations. *J. Atmos. Sci.,* **53,** 3710-3736.

Xu, K.-M., and coauthors, 2002: An intercomparison of cloud-resolving models with the ARM summer 1997 IOP data. *Q. J. Roy. Meteor. Soc.*, **128**, 593-624.

Xu, K.-M., and coauthors, 2005: Modeling springtime shallow frontal clouds with cloud-resolving and single-column models. *J. Geophys. Res.,* **110,** D15S04, doi: 10.1029/2004JD005153.

Xu, K.-M., T. Wong, B. A. Wielicki, and L. Parker, 2007: Statistical analysis of satellite cloud object data from CERES. Part IV. Boundary-layer cloud objects during 1998 El

Nino. *J. Climate,* (in press). [Available from http://asd-www.larc.nasa.gov/~tak/wong/f-publications.html].

Zhu, P., C.S. Bretherton, M. Köhler, A. Cheng, A. Chlond, Q. Geng, P. Austin, J.C. Golaz, G. Lenderink, A. Lock, and B. Stevens, 2005: Intercomparison and interpretation of single-column model simulations of a nocturnal stratocumulus-topped marine boundary layer. *Mon. Wea. Rev.,* **133,** 2741–2758.

List of Figures

Fig. 1. Time evolution of domain-averaged cloud fraction (%) from the IPHOC version of the CRM (a-e) and LES (f) for the BOMEX case. Horizontal grid-spacings of (a) 4 km, (b) 2 km, (c) 1 km, (d) 500 m, and (e) 250 m were used in the CRM simulations.

Fig. 2. Same as Fig. 1 [panels (a) - (e)] except for the LOC version of the CRM.

Fig. 3. Time series of the convective available potential energy (CAPE) from (a) the IPHOC and (b) the LOC versions of the CRM, and LES for the BOMEX case. Horizontal grid spacings ranging from 250 m to 4 km were used in the CRM simulations.

Fig. 4. Vertical transports of θ_l and q_t averaged over the last three hours of the LES and IPHOC simulations of the BOMEX case. The subgrid-scale transports ($\overline{w"\theta_l"}$, $\overline{w"q_t"}$) are shown in (a) and (c) while the resolved-scale transports ($\overline{w'\theta_l'}$, $\overline{w'q_t'}$) are shown in (b) and (d). The 3D-LES profiles are only shown in (a) and (c).

Fig. 5. Mean profiles of (a) liquid-water potential temperature, (b) total water mixing ratio, (c) cloud water content and (d) cloud fraction averaged over the last three hours of the BOMEX IPHOC and LES simulations. Horizontal grid sizes of 250 m, 500 m, 1 km, km and 4 km are used in the IPHOC simulations.

Fig. 6. Same as Fig. 5 except for the 1-km grid-spacing simulations with IPHOC and LOC versions of the CRM and the LES simulation.

Fig. 7. Time evolution of domain-averaged cloud fraction (%) from (a) LES, (b) IPHOC CRM and (c) LOC CRM for the ASTEX case. The 1-km grid spacing is used in both CRM simulations.

Fig. 8: Same as Fig. 5 except for the ASTEX case. The profiles were obtained from the averages over the last two hours of the IPHOC and LES simulations. The dots represent observations (Roode and Duynkerke 1997).

Fig. 9. Same as Fig. 4 except for the ASTEX case. The profiles were obtained from the averages over the last two hours of the IPHOC and LES simulations. The dots represent observations (Roode and Duynkerke 1997), which are better compared to the total fluxes.

Fig. 10. Same as Fig. 1 except for the ATEX case.

Fig. 11. Same as Fig. 2 except for the ATEX case.

Fig. 12. Same as Fig. 4 except for the ATEX case.

Fig. 13: Same as Fig. 5 except for the ATEX case.

-

Table 1: Summary of experiments performed in this study. The cloud-resolving model (CRM) with the low-order turbulence closure is denoted by LOC while the CRM with the intermediately-prognostic higher-order closure is denoted by IPHOC. CRM is run in 2D while the large-eddy simulation (LES) is run in 3D. See text for further details.

Experiment		Model	Number of grids	Grid Size	Hours
BOMEX	3D-LES	3D LES	64 × 64 × 75	100 m × 100 m × 40 m	6
	LOC 250 m	2D CRM with LOC	1024 x 75	250 m x 40 m	
	LOC 500 m		512 × 75	500 m × 40 m	
	LOC 1 km		256 × 75	1 km × 40 m	
	LOC 2 km		128 × 75	2 km × 40 m	
	LOC 4 km		64 × 75	4 km × 40 m	
	IPHOC 250 m	2D CRM with IPHOC	1024 x 75	250 m x 40 m	
	IPHOC 500 m		512 × 75	500 m × 40 m	
	IPHOC 1 km		256 × 75	1 km × 40 m	
	IPHOC 2 km		128 × 75	2 km × 40 m	
	IPHOC 4 km		64 × 75	4 km × 40 m	
ASTEX	3D-LES	3D LES	64 × 64 × 60	100 m × 100 m × 25 m	3
	LOC 250 m	2D CRM with LOC	1024 x 60	250 m x 25 m	
	LOC 500 m		512 × 60	500 m × 25 m	
	LOC 1 km		256 × 60	1 km × 25 m	
	LOC 2 km		128 × 60	2 km × 25 m	
	LOC 4 km		64 × 60	4 km × 25 m	
	IPHOC 250 m	2D CRM with IPHOC	1024 x 60	250 m x 25 m	
	IPHOC 500 m		512 × 60	500 m × 25 m	
	IPHOC 1 km		256 × 60	1 km × 25 m	
	IPHOC 2 km		128 × 60	2 km × 25 m	
	IPHOC 4 km		64 × 60	4 km × 25 m	
ATEX	3D-LES	3D LES	64 × 64 × 75	100 m × 100 m × 40 m	8
	LOC 250 m	2D CRM with LOC	1024 x 75	250 m x 40 m	
	LOC 500 m		512 × 75	500 m × 40 m	
	LOC 1 km		256 × 75	1 km × 40 m	
	LOC 2 km		128 × 75	2 km × 40 m	
	LOC 4 km		64 × 75	4 km × 40 m	
	IPHOC 250 m	2D CRM with IPHOC	1024 x 75	250 m x 40 m	
	IPHOC 500 m		512 × 75	500 m × 40 m	
	IPHOC 1 km		256 × 75	1 km × 40 m	
	IPHOC 2 km		128 × 75	2 km × 40 m	
	IPHOC 4 km		64 × 75	4 km × 40 m	

-

Figure 1. Time evolution of domain-averaged cloud fraction (%) from the IPHOC version of the CRM (a-e) and LES (f) for the BOMEX case. Horizontal grid-spacings of (a) 4 km, (b) 2 km, (c) 1 km, (d) 500 m, and (e) 250 m were used in the CRM simulations.

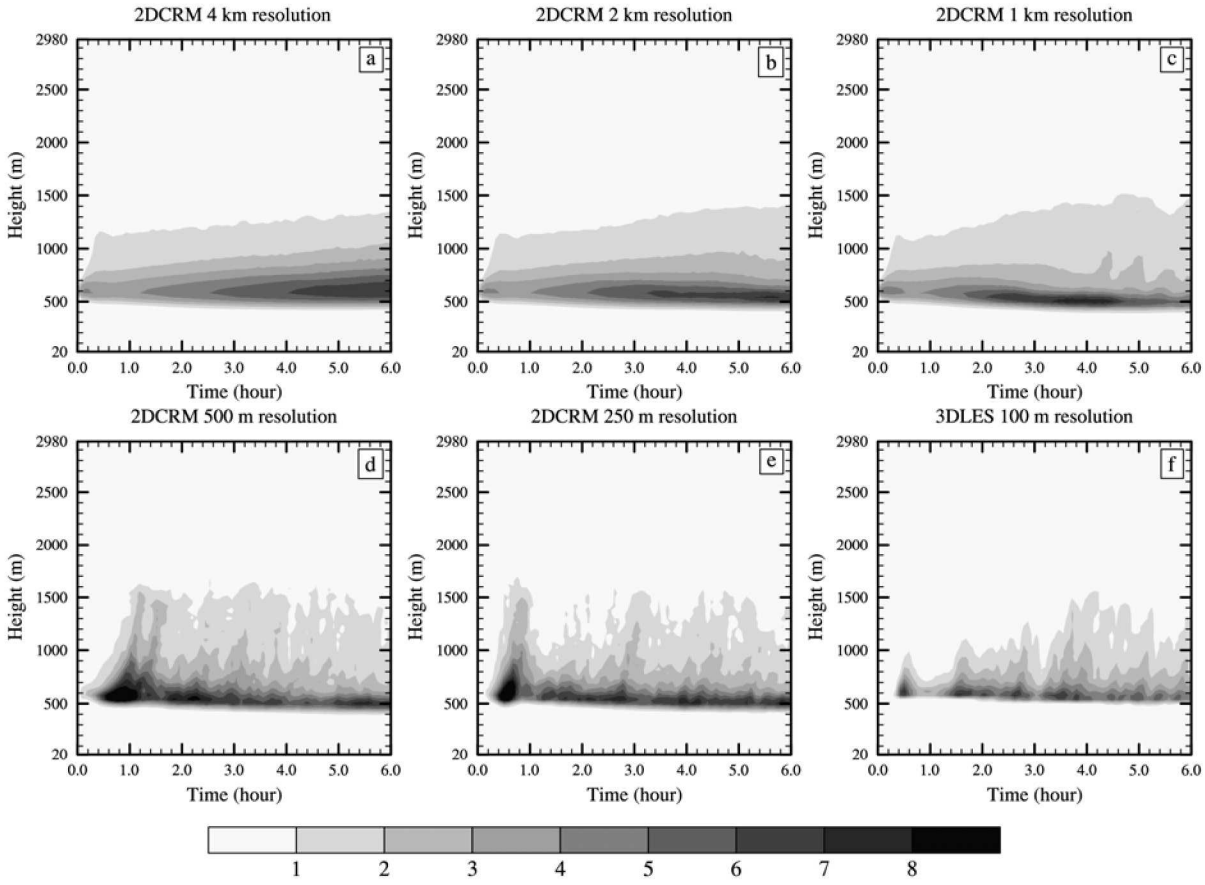

-

Figure 2. Same as Fig. 1 [panels (a) - (e)] except for the LOC version of the CRM.

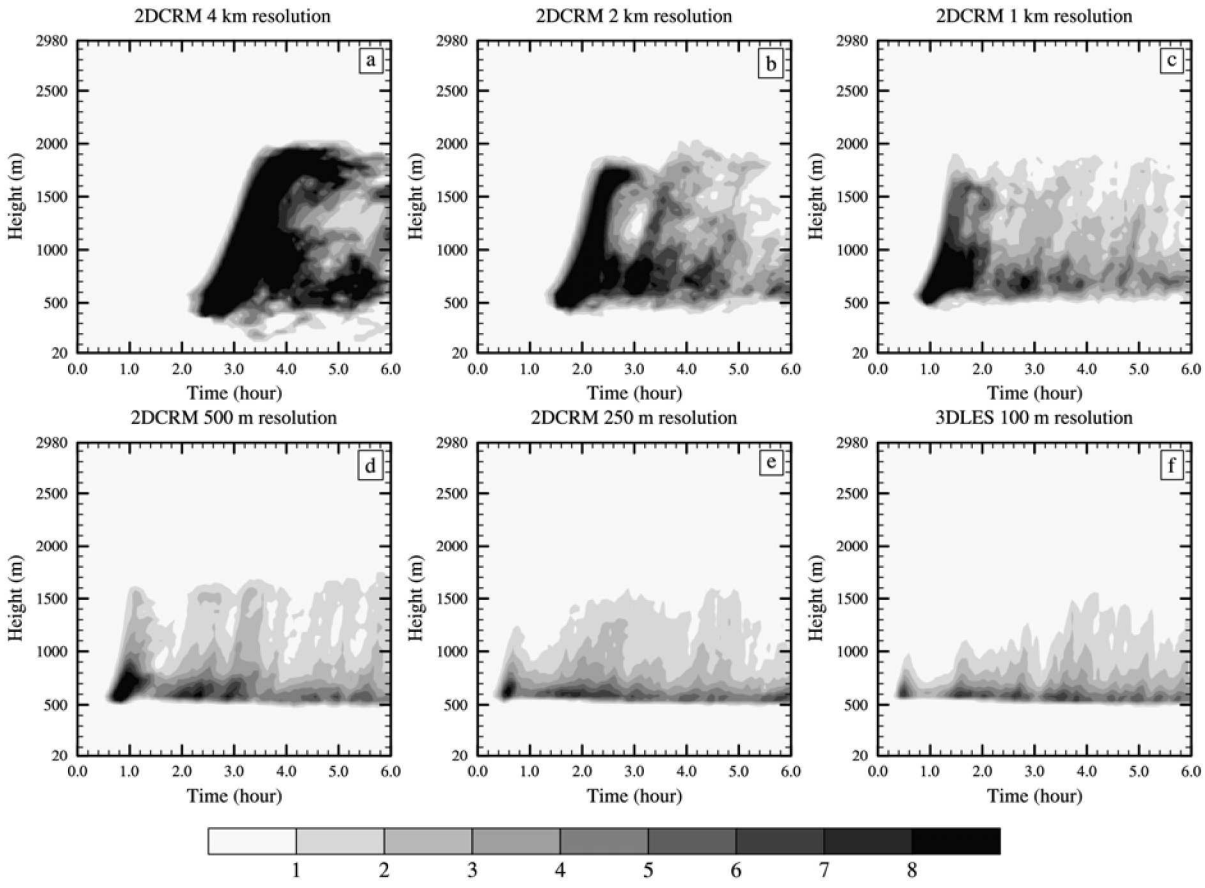

-

Figure 3. Time series of the convective available potential energy (CAPE) from (a) the IPHOC and (b) the LOC versions of the CRM, and LES for the BOMEX case. Horizontal grid spacings ranging from 250 m to 4 km were used in the CRM simulations.

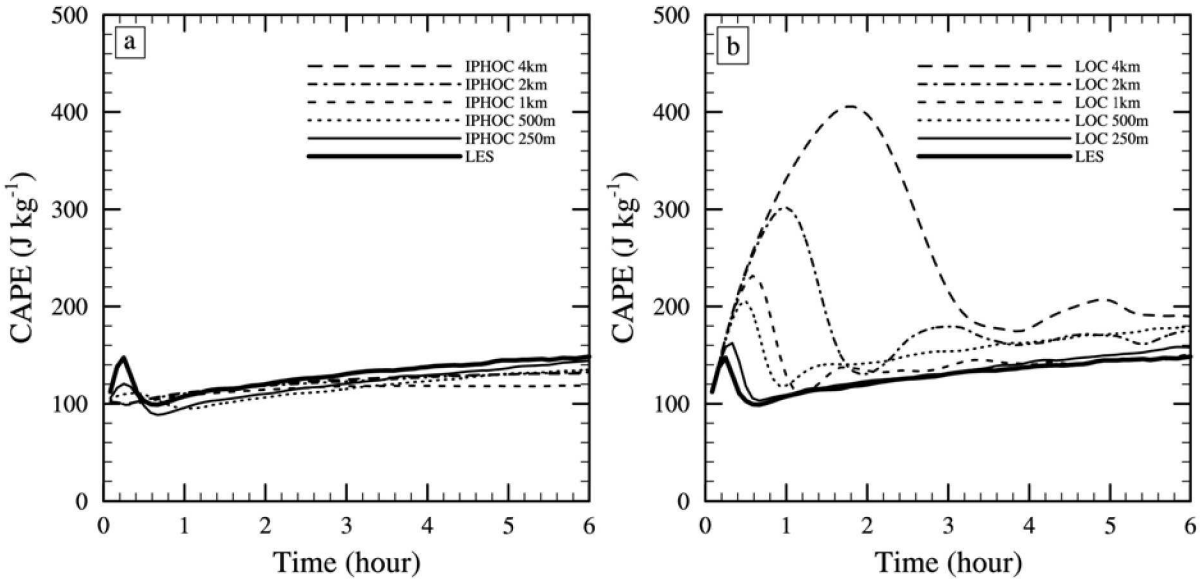

-

Figure 4. Vertical transports of θ_l and q_t averaged over the last three hours of the LES and IPHOC simulations of the BOMEX case. The subgrid-scale transports ($\overline{w''\theta_l''}$, $\overline{w''q_t''}$) are shown in (a) and (c) while the resolved-scale transports ($\overline{w'\theta_l'}$, $\overline{w'q_t'}$) are shown in (b) and (d). The LES profiles are only shown in (a) and (c).

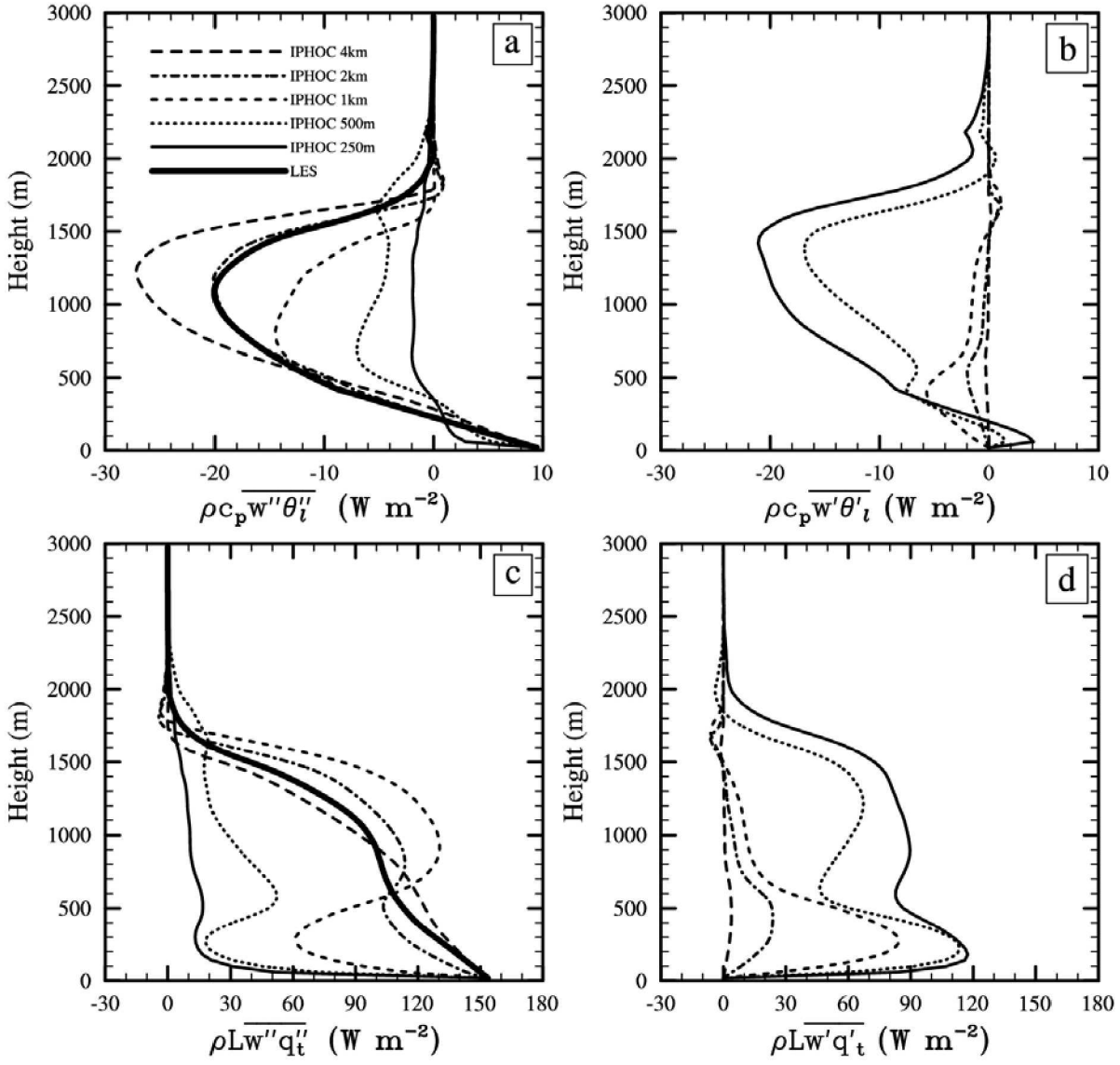

-

Figure 5. Mean profiles of (a) liquid-water potential temperature, (b) total water mixing ratio, (c) cloud water content and (d) cloud fraction averaged over the last three hours of the BOMEX IPHOC and LES simulations. Horizontal grid sizes of 250 m, 500 m, 1 km, km and 4 km are used in the IPHOC simulations.

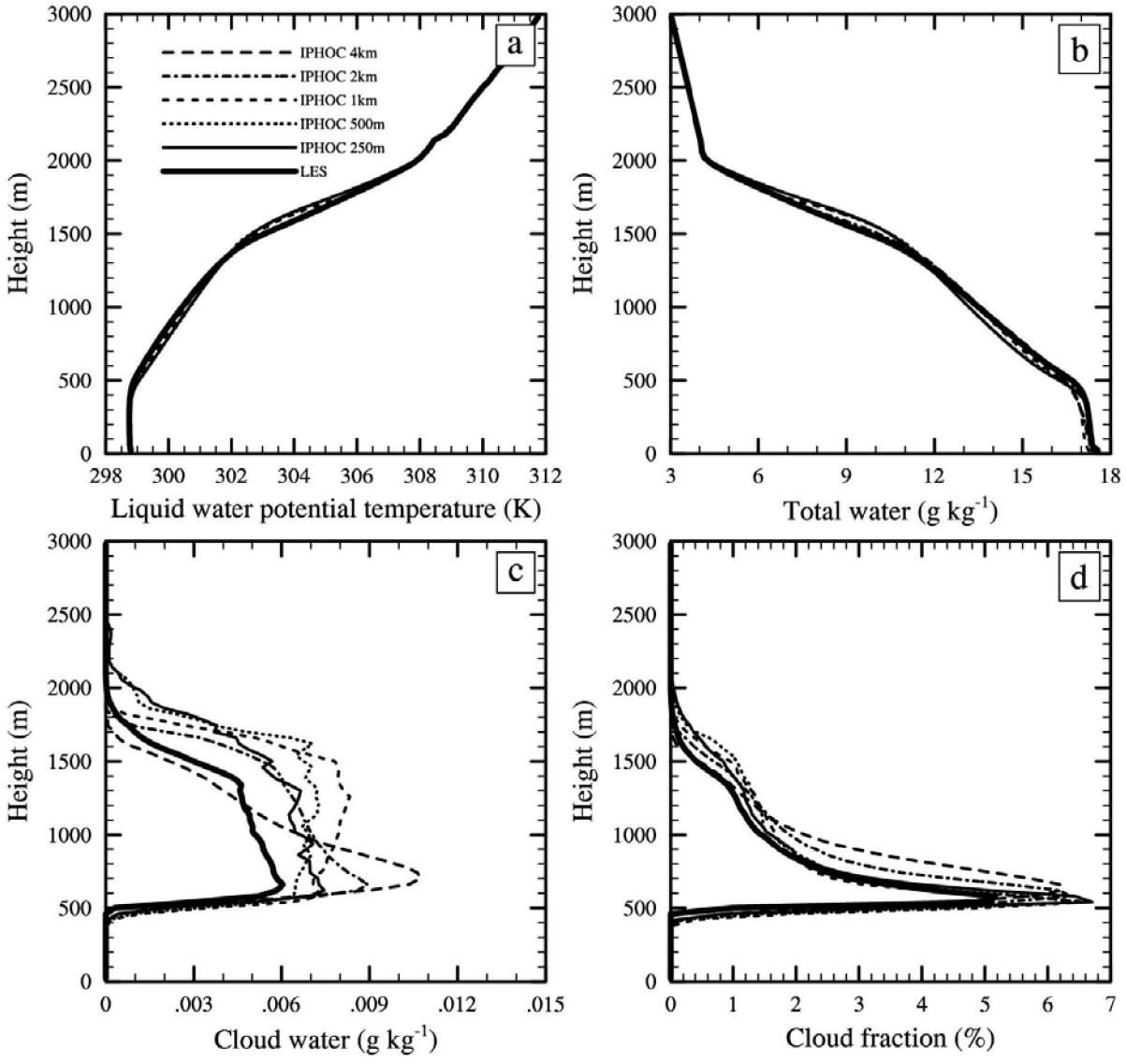

-

Figure 6. Same as Fig. 5 except for the 1-km grid-spacing simulations with IPHOC and LOC versions of the CRM and the LES simulation.

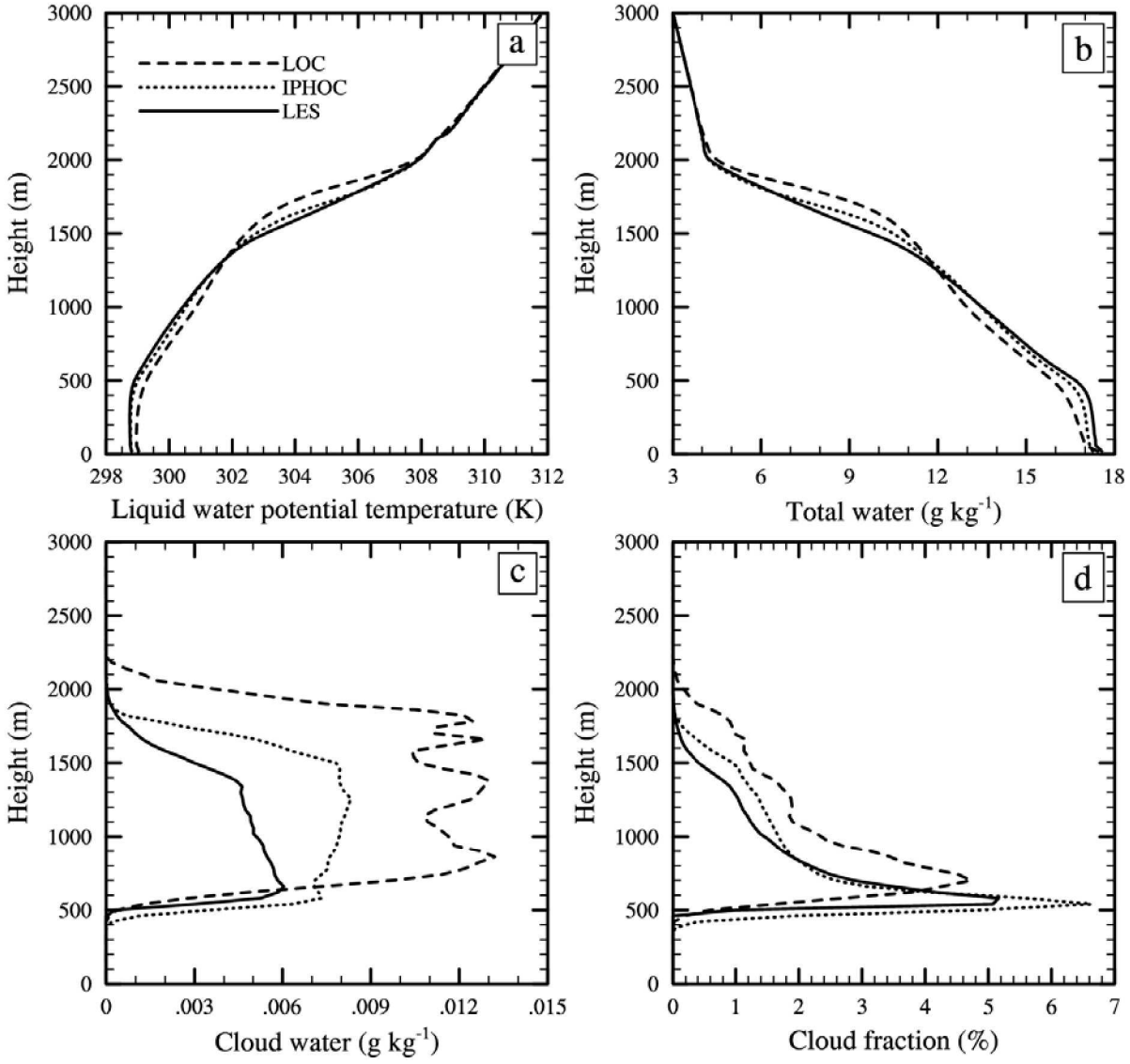

-

Figure 7. Time evolution of domain-averaged cloud fraction (%) from (a) LES, (b) IPHOC CRM and (c) LOC CRM for the ASTEX case. The 1-km grid spacing is used in both CRM simulations.

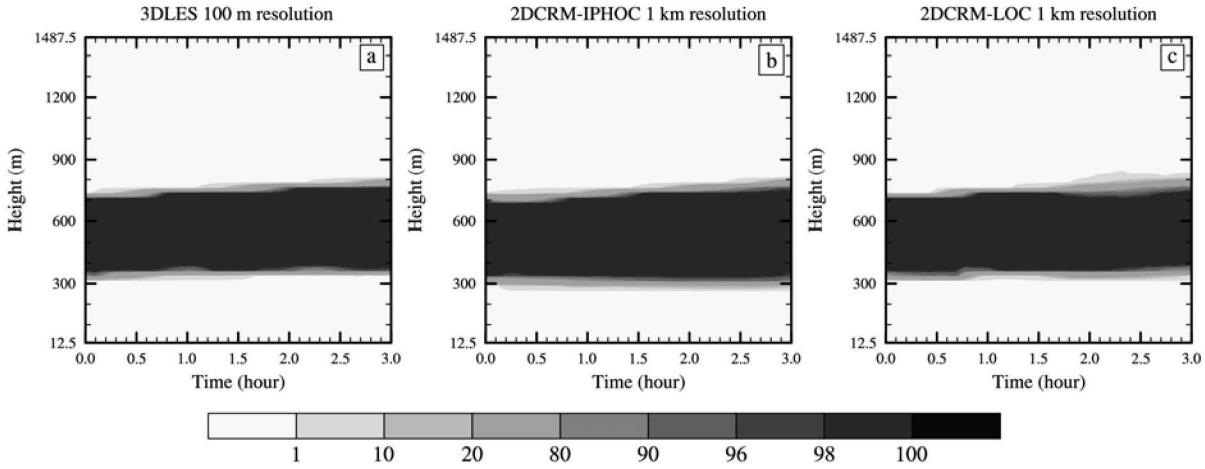

-

Figure 8. Same as Fig. 5 except for the ASTEX case. The profiles were obtained from the averages over the last two hours of the IPHOC and LES simulations. The dots represent observations (Roode and Duynkerke 1997).

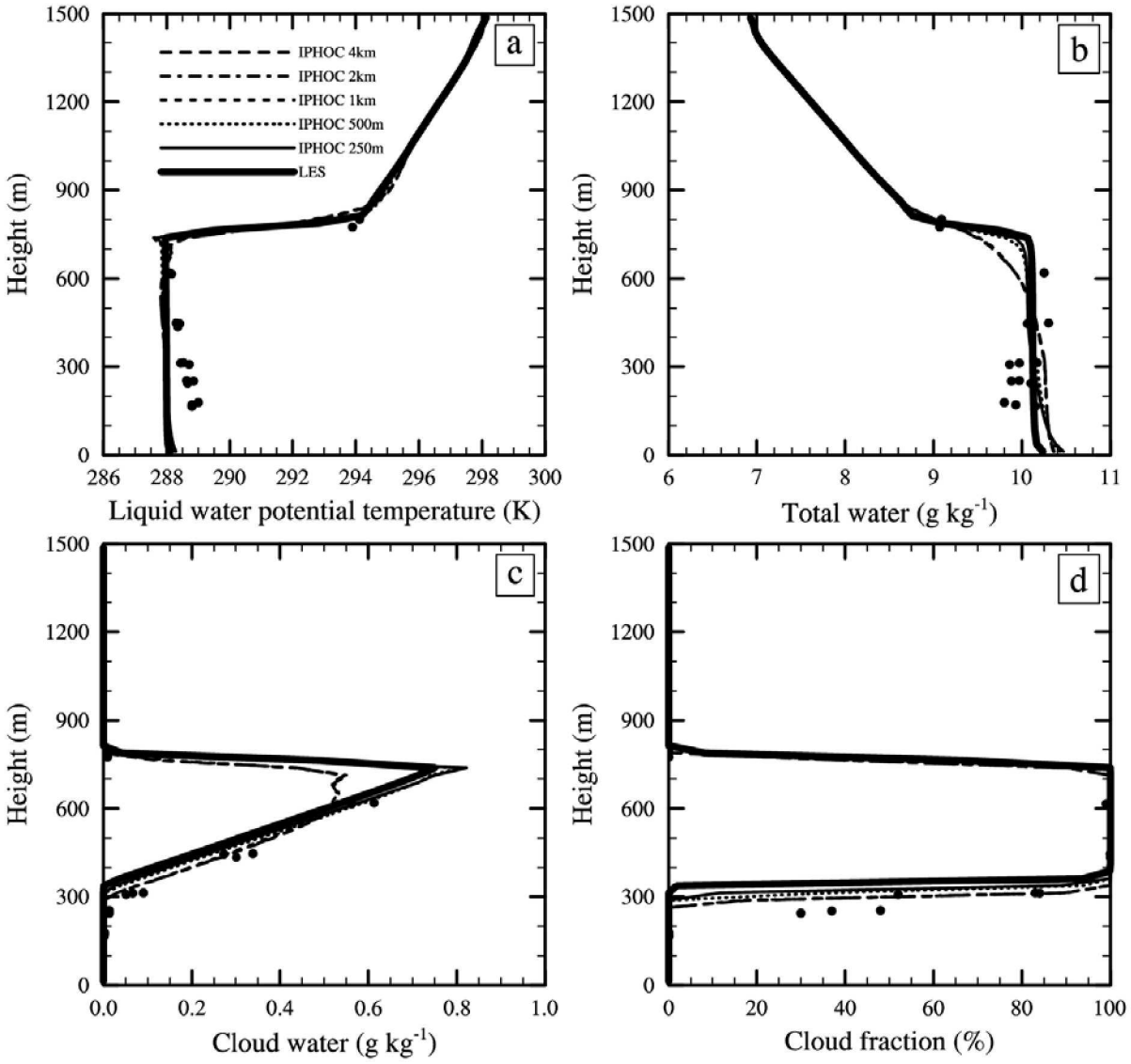

-

Figure 9. Same as Fig. 4 except for the ASTEX case. The profiles were obtained from the averages over the last two hours of the IPHOC simulations. The dots represent observations (Roode and Duynkerke 1997), which are better compared to the total fluxes.

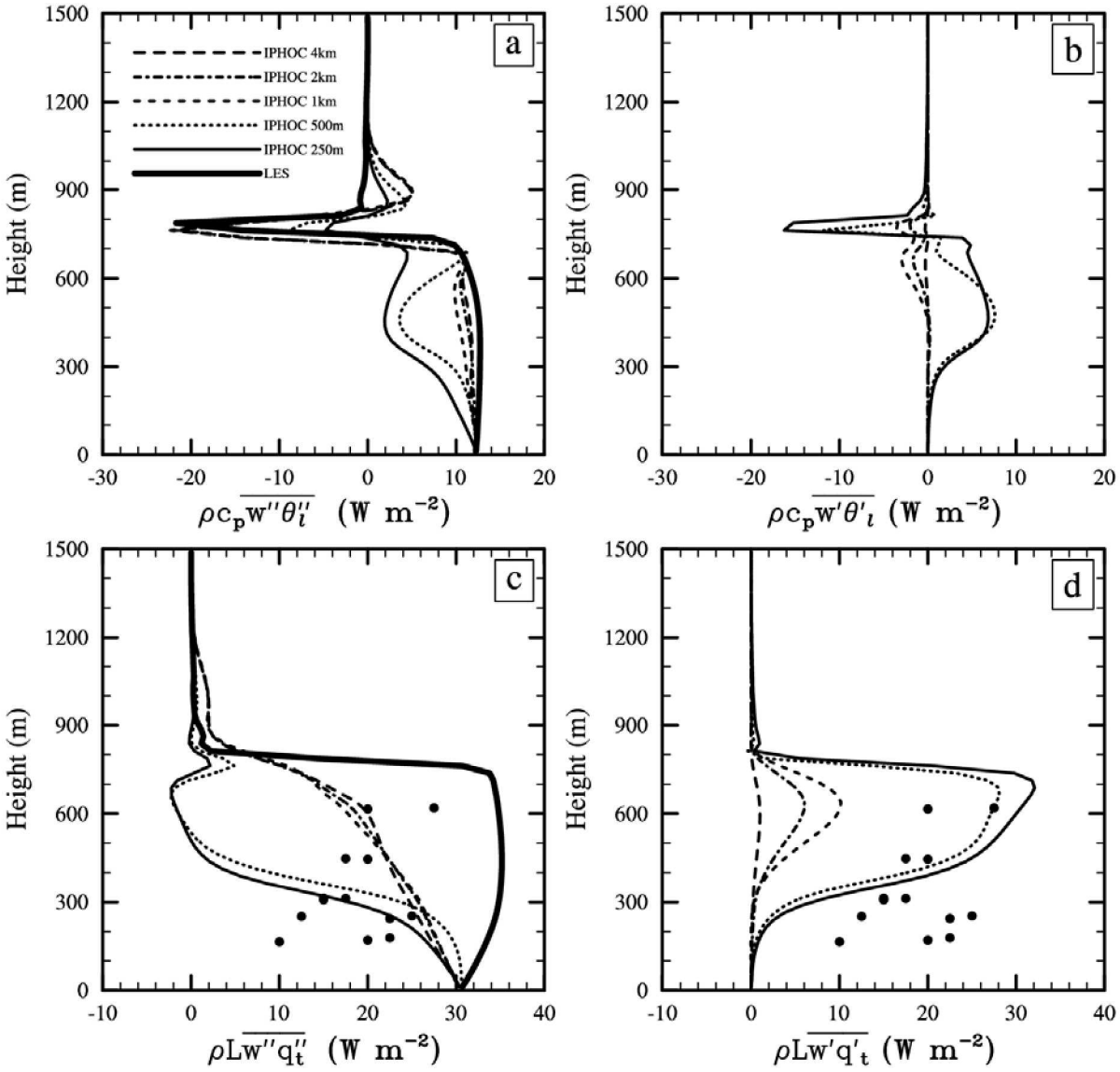

-

Figure 10. Same as Fig. 1 except for the ATEX case.

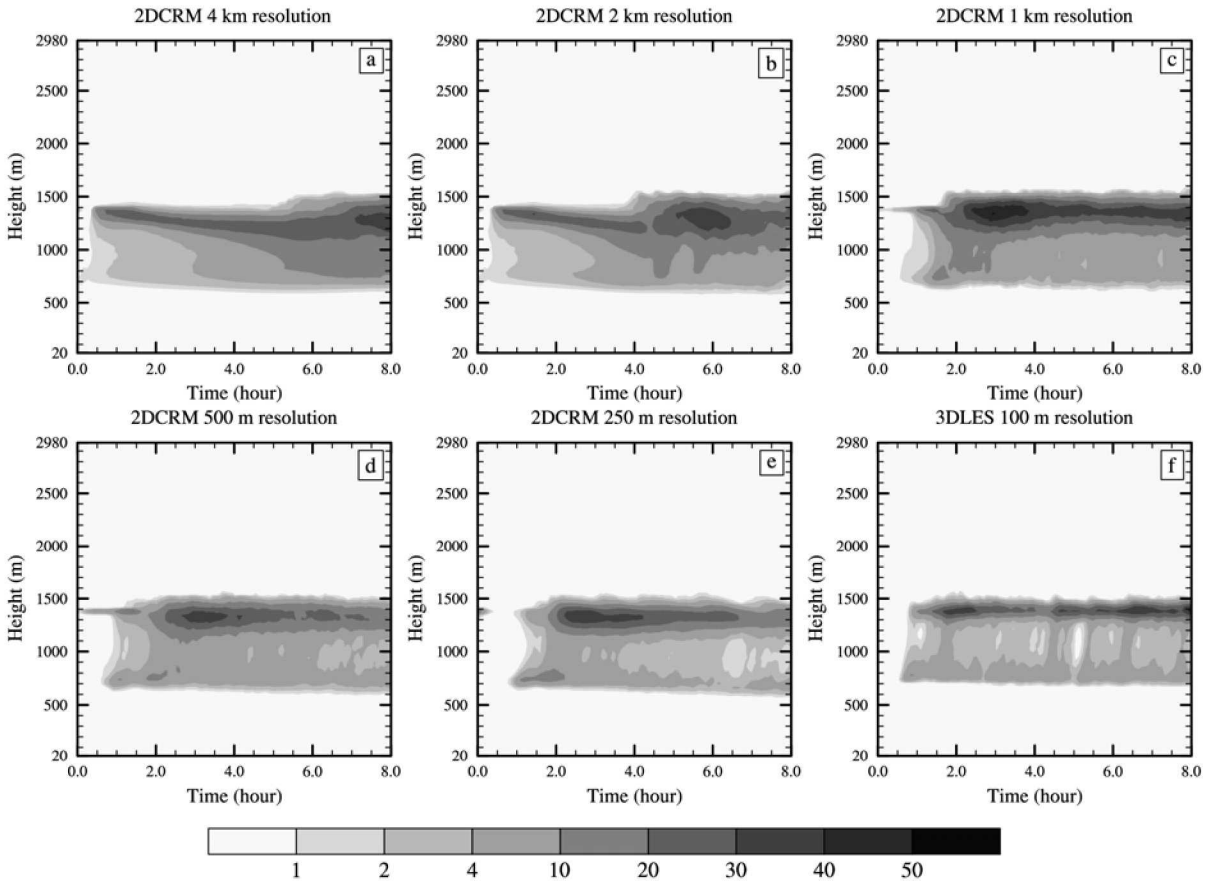

-

Figure 11. Same as Fig. 2 except for the ATEX case.

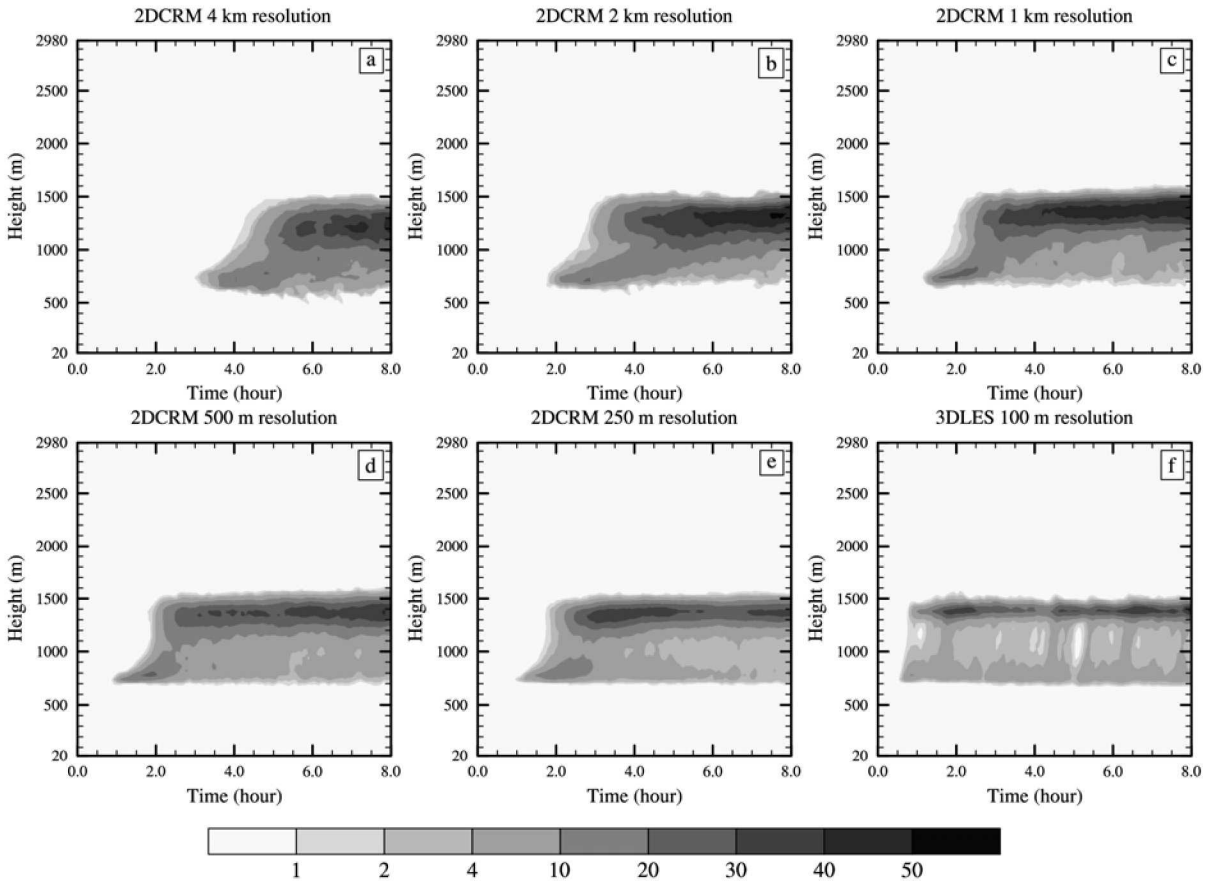

-

Figure 12. Same as Fig. 4 except for the ATEX case.

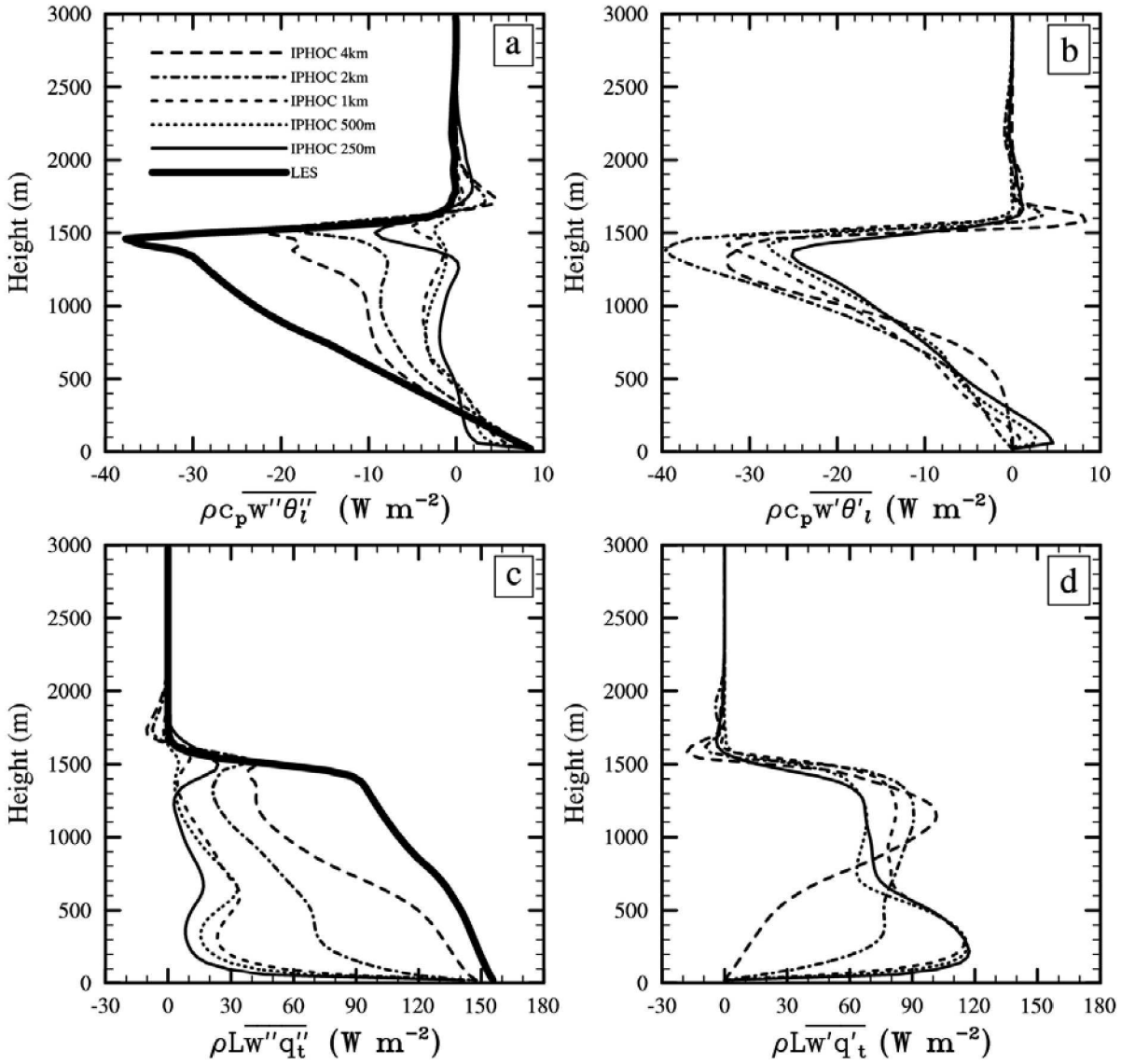

-

Figure 13: Same as Fig. 6 except for the ATEX case.